



Article

Dephosphorization in Double Slag Converter Steelmaking Process at Different Temperatures by Industrial Experiments

Han Sun ¹, Jian Yang ^{1,*}, Xinwu Lu ², Wanshan Liu ², Gefan Ye ¹, Runhao Zhang ¹  and Wenkui Yang ¹ 

¹ State Key Laboratory of Advanced Special Steel, School of Materials Science and Engineering, Shanghai University, Shanghai 200444, China; sun_han@shu.edu.cn (H.S.); ye_gefan@shu.edu.cn (G.Y.); zhangrunhao@shu.edu.cn (R.Z.); yangwenkui@shu.edu.cn (W.Y.)

² Ningbo Iron and Steel Group Co., Ltd., Ningbo 315807, China; luxinwu@ningbosteel.com (X.L.); liuwanshan@ningbosteel.com (W.L.)

* Correspondence: yang_jian@t.shu.edu.cn; Tel.: +86-21-6613-6580

Abstract: In the present work, the effect of dephosphorization endpoint temperature on the dephosphorization of hot metal was studied for the double slag converter steelmaking process under the conditions of low temperature and low basicity by the industrial experiments. In the temperature range of 1350–1450 °C, with an increasing dephosphorization endpoint temperature, the dephosphorization ratio and phosphorus distribution ratio first increase and then decrease. The phosphorus content in hot metal first decreases and then increases at the end of dephosphorization. At the dephosphorization temperature range of 1385–1410 °C, the dephosphorization ratio is higher than 55%, the P₂O₅ content in the dephosphorization slag is 3.93–4.17%, the logL_P value is 1.76–2.09, the value of P_{CO}^{P-C} of the selective oxidation reaction of carbon and phosphorus is 53–80 Pa, and the a_{FeO} value is 0.284–0.312. The path of phosphorus in hot metal entering the P-rich phase of dephosphorization slag can be reasonably inferred as: hot metal → Fe-rich phase → P-rich phase. Under the present industrial experimental conditions, the dephosphorization and rephosphorization reactions are in dynamic equilibrium at 1413 °C. Considering the experimental results and thermodynamic calculation results of industrial experiments by the double slag dephosphorization process, the optimal temperature range for intermediate deslagging is about 1400–1420 °C.

Keywords: double slag converter steelmaking process; hot metal dephosphorization; dephosphorization endpoint temperature; dephosphorization ratio; phosphorus distribution ratio; optimum temperature of intermediate deslagging



Citation: Sun, H.; Yang, J.; Lu, X.; Liu, W.; Ye, G.; Zhang, R.; Yang, W. Dephosphorization in Double Slag Converter Steelmaking Process at Different Temperatures by Industrial Experiments. *Metals* **2021**, *11*, 1030. <https://doi.org/10.3390/met11071030>

Academic Editor: Pasquale Cavaliere

Received: 17 May 2021

Accepted: 21 June 2021

Published: 26 June 2021

Publisher's Note: MDPI stays neutral with regard to jurisdictional claims in published maps and institutional affiliations.



Copyright: © 2021 by the authors. Licensee MDPI, Basel, Switzerland. This article is an open access article distributed under the terms and conditions of the Creative Commons Attribution (CC BY) license (<https://creativecommons.org/licenses/by/4.0/>).

1. Introduction

The double slag converter steelmaking process developed by Nippon Steel in 2001 is the most representative, which is called Multi-Refining Converter (MURC) [1]. In this process, the desiliconization and dephosphorization operations are performed in the converter firstly, and the dephosphorization slag is poured out by tilting furnace. Then, the decarburization operation is performed in the same converter and the decarburization slag is left in the converter for reusing in the next charge.

Some scholars have carried out researches on the double slag converter steelmaking process by industrial experiments. Yang Wang et al. [2]. conducted the double slag converter steelmaking process by using a low oxygen lance height in the dephosphorization stage of the industrial converter. The stirring of molten steel is strengthened, and the phosphorus content is reduced at the end of decarburization from an average value of 0.018% to an average value of 0.011%, and the dephosphorization ratio is increased by more than 6%. He Wu et al. [3]. conducted the industrial experiments and showed that the average dephosphorization ratio of 62.2% and the average phosphorus content of 0.048% can be achieved under the process conditions of the lower temperature of 1330–1350 °C, the bottom blowing stirring intensity of 0.03–0.04 m³/t·min, the medium slag basicity of 2.0–3.0

and the high iron oxide content of 20–25%. Our previous experimental results [4] showed that with increasing the basicity of dephosphorization slag, the phosphorus distribution ratio and dephosphorization ratio increase, and the area fraction of phosphorus rich phase in dephosphorization slag increases with the increasing area fraction of iron-rich phase.

In the hot metal dephosphorization reaction, the slag is in the state of solid–liquid multiphase coexistence. While lime dissolves, $2\text{CaO}\cdot\text{SiO}_2$ (C_2S) is formed [5]. C_2S tends to combine with $3\text{CaO}\cdot\text{P}_2\text{O}_5$ (C_3P) in liquid slag to form solid solution $2\text{CaO}\cdot\text{SiO}_2\text{-}3\text{CaO}\cdot\text{P}_2\text{O}_5$ ($\text{C}_2\text{S-C}_3\text{P}$) [6,7]. Kitamura et al. [8] found that the mass transfer of CaO and SiO_2 occurs simultaneously with the mass transfer of P_2O_5 . Xie et al. [9] found that the diffusion of phosphorus from the $\text{C}_2\text{S-C}_3\text{P}$ solid solution reaction layer to the internal encapsulated C_2S is the rate-controlling step of phosphorus transport. Kakimoto et al. [10] found that the thickness of the FeO-CaO layer is related to the thickness of the C_2S phase. Wu et al. [11] found that almost all the phosphorus in $\text{CaO-FeO-SiO}_2\text{-MgO-MnO-Al}_2\text{O}_3\text{-P}_2\text{O}_5\text{-TiO}_2$ slag with the basicity close to 3 is combined with C_2S but not with $3\text{CaO}\cdot\text{SiO}_2$ (C_3S), and C_2S crystal grows uniformly into a spherical shape. Pahlevani et al. [12] found that the distribution ratio of phosphorus in solid solution and liquid slag is determined by the CaO content in liquid slag and activity coefficient of P_2O_5 in solid solution.

The effect of temperature on dephosphorization in the double slag converter steel-making process was one of the most important points for a highly efficient implementation of this process. Tian et al. [13] found that when the Fe^{3+} content in slag is between 2.33 and 5.98%, the basicity is between 1.72 and 3.14, and the temperature is between 1600 and 1700 °C, the dephosphorization ratio gradually decreases with increasing temperature. Yang et al. [14] found that in the temperature range of 1600–1660 °C, with increasing temperature, the phosphorus distribution ratio gradually decreases, the endpoint phosphorus content increases, and the dephosphorization ratio decreases. Zhou et al. [15] found that in the temperature range of 1590–1640 °C, the total rephosphorization content of molten steel first decreases and then increases. From the above literature, it can be seen that the effect of temperature on converter dephosphorization mainly focused on the endpoint temperature of converter decarburization, ranging from 1590 to 1700 °C; there were few reports on the temperature range of 1350–1450 °C.

The effect of the oxygen potentials at the different reaction interfaces on dephosphorization was also studied. Han et al. [16] concluded that when the dissolved oxygen content in the endpoint molten steel is between 0.03% and 0.045%, the $[\text{P}]\text{-}[\text{O}]$ equilibrium phosphorus content is 21–38 times that of $[\text{P}]\text{-}(\text{FeO})$ equilibrium phosphorus content. Kitamura et al. [17] found that the oxygen activity of the FeO phase in dephosphorization slag is two orders of magnitude larger than that of equilibrium oxygen activity in hot metal containing more than 4% of carbon.

In addition, some scholars have studied the optimum deslagging temperature of dephosphorization slag in the double slag converter steelmaking process. Based on the selective oxidation reaction of carbon and phosphorus, Wu et al. [4] calculated the carbon–phosphorus selective oxidation transition temperature to be 1342 °C according to the dephosphorization slag compositions and semi-steel control target, and they took it as the guiding temperature for dephosphorization slag deslagging. Chaogang Zhou et al. [18] calculated the optimal deslagging temperature of dephosphorization slag and obtained that the equilibrium temperature of dephosphorization in the early stage of converter blowing is 1435 °C.

According to the above literatures, it can be seen that in the research of the double slag converter steelmaking process, the effect of dephosphorization endpoint temperature in the range of 1350–1450 °C on hot metal dephosphorization is rarely studied. Since the lower temperature range of 1350–1450 °C and the lower basicity of range about 1.5–1.6 are the main process range for the dephosphorization in the double slag converter steelmaking process, it is necessary to clarify the effect of the dephosphorization endpoint temperature on hot metal dephosphorization.

In this paper, through the 180 t double slag converter steelmaking industrial experiments, the effect of the dephosphorization endpoint temperature on the dephosphorization was studied at the low basicity slag in the relatively low temperature range of 1350–1450 °C. In addition, XRD and SEM-EDS were used to study the phase species and phase compositions of dephosphorization slag under the optimal dephosphorization ratio, and the enrichment path of phosphorus in dephosphorization slag was reasonably speculated. The effect of dephosphorization endpoint temperature on the oxygen activity at different reaction interfaces was analyzed. The phosphorus capacity and phosphorus distribution ratio of slag were calculated and compared with the empirical formula of the previous scholars. The optimum deslagging temperature of dephosphorization slag was further analyzed.

2. Experimental Procedure

2.1. Double Slag Converter Steelmaking Experiments

The industrial experiment was carried out with a 180 t converter in the steelmaking plant of Ningbo Iron and Steel Co. Ltd., Ningbo, China. Figure 1 shows the flow chart of the double slag converter steelmaking process, and the double slag converter steelmaking process is mainly divided into eight steps.

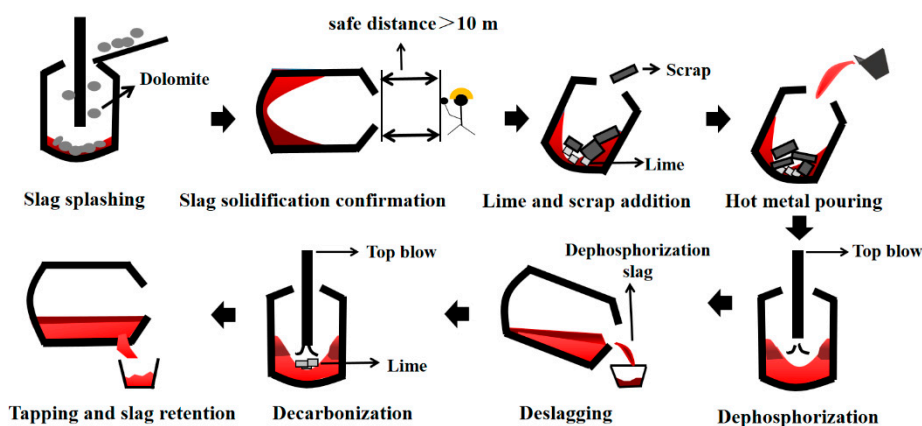


Figure 1. Flow chart of double slag converter steelmaking process.

After adding light burned dolomite as a slag-adjusting agent, slag splashing was carried out to protect the furnace wall. The added auxiliary materials included lime, magnesite, sinter, OG (Oxygen converter Gas recovery) slag pellets, etc. The OG slag pellets contained 55% T.Fe, 12.4% CaO, and 3.8% SiO₂, and they mainly include the mud produced by oxygen converter gas recovery. “T.Fe” refers to the total content of iron element in slag, (mass%). In addition, about 20 mass% of iron oxide scale, 13 mass% of lime, 2 mass% of binder, and 65 mass% of OG mud are molded by a high-pressure ball pressing machine and then dried at low temperature to form OG slag pellets, which can regulate converter temperature and promote rapid slag formation.

After confirming the solidification of the slag, the active lime and the scrap steel is added at first; then, the hot metal is poured into the furnace. Finally, an oxygen lance is ignited for dephosphorization and a low–high–low lance position is used in the dephosphorization stage. The initial low lance position aims to promote the ignition of the oxygen blowing. The subsequent high lance position is to promote the formation of molten slag in the early stage of dephosphorization and to increase the T.Fe content in slag. At the later stage of dephosphorization, the low lance position is used to promote dephosphorization. After the dephosphorization stage is completed, the dephosphorization slag is poured out by tilting the furnace, and then lime, dolomite, and other auxiliary materials are added for decarburization. After the decarburization, the molten steel is tapped out, and the decarburization slag is left in the furnace for the dephosphorization in the next charge.

2.2. Compositions of the Initial Hot Metal, the Hot Metal at the Endpoint of Dephosphorization, and Dephosphorization Slag

The compositions and temperatures of the initial hot metal in the converter are shown in Table 1. The number of experimental heats is T1350~T1450, which is used as the number of subsequent hot metal samples at the endpoint of dephosphorization and the dephosphorization slag samples. The hot metal after desulfurization is used for dephosphorization, and the temperature of the initial hot metal charged into the furnace is in the range of 1326–1366 °C. The added amount of the initial hot metal is 190–195 t, and the added amount of scrap steel is 20–30 t.

Table 1. The compositions and temperatures of the initial hot metal in converter (mass%).

Sample	C	Si	Mn	S	P	T/°C
T1350	4.65	0.29	0.18	0.03	0.145	1330
T1360	4.65	0.36	0.25	0.01	0.162	1326
T1370	4.65	0.34	0.29	0.03	0.148	1350
T1385	4.65	0.32	0.29	0.01	0.157	1350
T1395	4.65	0.41	0.28	0.01	0.141	1365
T1405	4.65	0.29	0.27	0.01	0.129	1366
T1410	4.65	0.31	0.25	0.02	0.136	1357
T1420	4.65	0.40	0.31	0.04	0.135	1355
T1450	4.65	0.39	0.29	0.03	0.158	1365

After the dephosphorization reaction, the slag sample is taken by sticking onto an iron rod and cooling in air. After grinding, the slag sample was passed through a 200-mesh sieve to remove the residual iron particles remaining in the slag. The compositions of slag samples were analyzed with an M4 TORNADO fluorescence spectrometer of Bruker Company in Germany. The temperature was measured, the hot metal was sampled with a sub-gun, and the compositions of hot metal were analyzed by SPECTROMAXx direct reading spectrometer of German SPECTRO Company. Before the analyses, the spectrometer was calibrated with the standard samples of the similar compositions.

Table 2 shows hot metal compositions, dephosphorization ratios, and temperatures at the endpoint of dephosphorization. Table 3 shows dephosphorization slag compositions and basicities at the endpoint of dephosphorization. It can be seen from Table 2 that the temperature of the dephosphorization endpoint is in the range of 1350–1450 °C. Basicity B is calculated with Equation (1), and η_P represents the dephosphorization ratio, which is calculated by Equation (2) [19]:

$$B = \frac{(\%CaO)}{(\%SiO_2)} \quad (1)$$

$$\eta_P = \frac{[\%P]_0 - [\%P]_e}{[\%P]_0} \times 100\% \quad (2)$$

(%CaO) and (%SiO₂) are the mass percentages of CaO and SiO₂ in the dephosphorization slag respectively, [%P]₀ is the initial phosphorus content in initial hot metal, and [%P]_e is the phosphorus content in the hot metal at the end of dephosphorization.

The phase analysis of dephosphorization slag was carried out by a D8 Advance X-ray powder diffractometer (XRD) of Bruker company in Germany. In the range of 2θ = 10–90° and step size of 0.04° s⁻¹, XRD data were collected by Cu-Kα radiation. A small amount of massive dephosphorization slag was embedded in epoxy resin. After solidification, it was ground and polished by an automatic grinding and polishing machine of the PRESI company in France. Then, the surface was carbonized by a magnetron sputtering MC1000 of the HITACHI company in Japan. The morphology of the P-rich phase of dephosphorization slag was observed by a Zeiss EVO 18 electronic scanning microscope of Zeiss company of Germany, and the chemical composition of the P-rich phase in dephosphorization slag was

analyzed by an X-MaxN large area energy-dispersive spectrometer (SEM-EDS) of Oxford Instruments Company in the UK.

Table 2. Hot metal compositions, dephosphorization ratios, and temperatures at the end of dephosphorization (mass%).

Sample	C	Si	Mn	S	P	$\eta_p/\%$	$T/^\circ\text{C}$
T1350	3.076	0.010	0.060	0.018	0.073	49.7	1350
T1360	3.081	0.025	0.089	0.010	0.080	50.6	1360
T1370	3.241	0.015	0.097	0.009	0.071	52.0	1370
T1385	3.039	0.010	0.092	0.010	0.069	56.1	1385
T1395	3.069	0.022	0.117	0.018	0.050	64.5	1395
T1405	2.942	0.009	0.167	0.018	0.034	73.6	1405
T1410	2.943	0.012	0.143	0.017	0.051	62.5	1410
T1420	3.253	0.017	0.138	0.012	0.069	48.9	1420
T1450	3.488	0.015	0.147	0.019	0.103	34.8	1450

Table 3. Compositions and basicities of dephosphorization slag (mass%).

Sample	CaO	SiO ₂	MgO	MnO	Al ₂ O ₃	P ₂ O ₅	FeO	B/-
T1350	35.96	22.77	7.24	9.37	2.52	3.17	18.97	1.58
T1360	34.87	21.53	9.05	9.76	2.56	3.85	18.38	1.62
T1370	34.66	22.51	8.15	9.25	2.83	3.73	18.87	1.54
T1385	35.22	21.60	8.58	10.01	3.59	3.96	17.04	1.63
T1395	34.88	22.48	8.98	9.92	2.86	3.93	16.95	1.55
T1405	37.30	22.71	8.23	8.49	2.27	4.17	16.83	1.64
T1410	35.73	22.91	8.94	8.29	3.05	3.95	17.13	1.56
T1420	35.51	23.71	9.18	8.80	2.85	3.57	16.38	1.50
T1450	35.28	23.84	9.35	8.59	2.23	3.17	17.54	1.48

3. Results

3.1. Effect of Dephosphorization Endpoint Temperature on Liquidus Region of Dephosphorization Slag

Figure 2 shows the effect of dephosphorization endpoint temperature on liquidus regions of the CaO-SiO₂-FeO-10%MgO-10%MnO-5%P₂O₅ dephosphorization slag. The liquidus projection section of dephosphorization slag at 1340–1460 °C was drawn by a phase diagram in Factsage7.3. Figure 2 shows that with increasing dephosphorization endpoint temperature, the liquid phase area of dephosphorization slag increases continuously, and the slag can be melted better. At the same time, the dephosphorization slag selected in the present work is marked in Figure 2 by using the ternary phase diagram of CaO, SiO₂, and FeO. Since the selected dephosphorization slags are from the different heats of the double slag converter steelmaking experiment, the basicities of dephosphorization slag are slightly different. Nine groups of dephosphorization slag components all located in red quadrilateral area indicate that the difference in the basicities of these dephosphorization slags is quite small. Therefore, it can be considered that the experimental results are mainly affected by the dephosphorization endpoint temperature.

3.2. Effect of Dephosphorization Endpoint Temperature on Dephosphorization

In industrial experiments, it is difficult to ensure that the other process parameters are the same to investigate the effect of dephosphorization endpoint temperature on hot metal dephosphorization. In the heats selected in the present work, the slag basicities ranged from 1.48 to 1.64, and the FeO contents in slag were from 16.38% to 18.97%. The MgO contents in slag from 7.24% to 9.35% increased with the increasing dephosphorization endpoint temperature, which was mainly caused by the erosion of the converter wall. The contents of CaO, SiO₂, MnO, and Al₂O₃ in the dephosphorization slag changed very little.

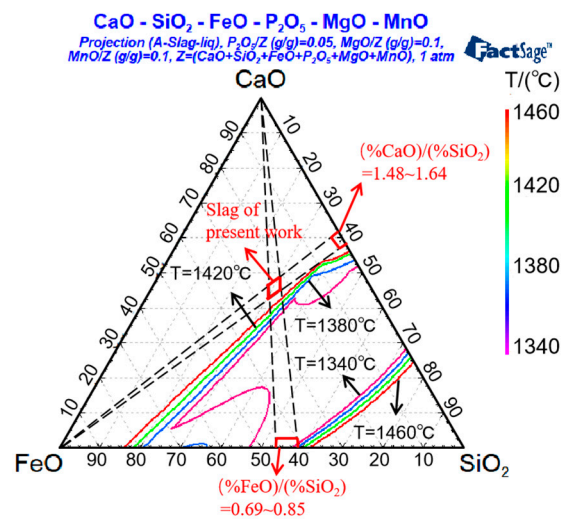


Figure 2. Effect of dephosphorization endpoint temperature on liquidus regions of the CaO-SiO₂-FeO-10%MgO-10%MnO-5%P₂O₅ dephosphorization slag.

Figure 3 shows the effect of dephosphorization endpoint temperature on the dephosphorization ratio, phosphorus content in hot metal, and P₂O₅ content in dephosphorization slag at the endpoint of dephosphorization. When the dephosphorization endpoint temperature is 1350–1385 °C, the dephosphorization ratio is between 49.7 and 56.1%. The phosphorus content and dephosphorization ratio in hot metal have no obvious change in this range. When the dephosphorization endpoint temperature is increased to 1385–1405 °C, the dephosphorization ratio increases significantly. At 1405 °C, the dephosphorization ratio reaches the highest value of 73.64% and the phosphorus content in hot metal reduces to the lowest value of 0.034%. This is because when the dephosphorization endpoint temperature is relatively low in the temperature range of 1350–1385 °C, although the thermodynamic condition is beneficial to dephosphorization, the lime cannot be well melted during the very short time period of about 5 min during the dephosphorization period in the double slag converter steelmaking process. Therefore, the poor kinetic conditions hindered the dephosphorization reaction. When the temperature is in the range of 1385–1405 °C, the auxiliary materials in the converter are well melted, the slagging is improved, and the dephosphorization thermodynamic conditions can still promote the dephosphorization of the converter, so the dephosphorization ratio is significantly increased in this range.

In the dephosphorization endpoint temperature range of 1350–1405 °C, the content of P₂O₅ in the dephosphorization slag increases with the increasing dephosphorization endpoint temperature and the content of P₂O₅ in the dephosphorization slag is relatively high, which is from 3.17% to 4.17%. This is because with the increasing dephosphorization endpoint temperature, the lime begins to melt, and the kinetic conditions of the reaction between molten slag and hot metal are improved, so that the initial dephosphorization capacity increases. When the dephosphorization endpoint temperature is 1405 °C, the P₂O₅ content reaches the maximum value of 4.17%.

When the dephosphorization endpoint temperature is further increased to higher than 1405 °C, the dephosphorization ratio of hot metal is decreased, the phosphorus content at the endpoint of dephosphorization is increased, and the content of P₂O₅ in the dephosphorization slag decreases. The reason is that the dephosphorization reaction is exothermic, and the high temperature will inhibit the dephosphorization reaction. Although the slagging is promoted and the kinetic conditions of dephosphorization in the converter are improved, too high temperature has a greatly adverse effect on the thermodynamic conditions of dephosphorization, leading to a great decrease in the equilibrium constant of dephosphorization reaction. Therefore, the thermodynamic and kinetic conditions of dephosphorization jointly determine the dephosphorization ratio.

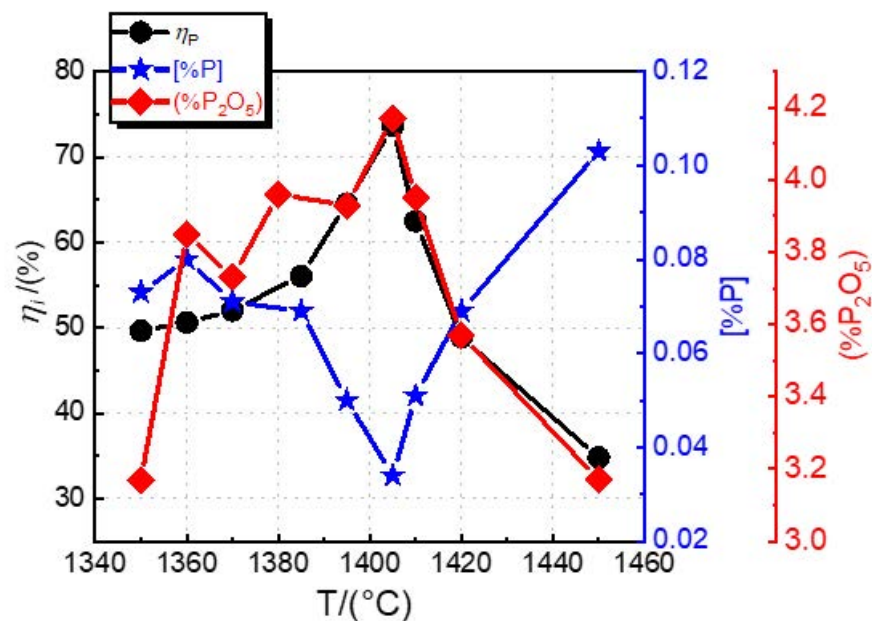


Figure 3. Effect of dephosphorization endpoint temperature on the dephosphorization ratio, phosphorus content in hot metal, and P₂O₅ content in dephosphorization slag at the endpoint of dephosphorization.

According to the results of Figure 3, when the dephosphorization endpoint temperature is between 1385 and 1410 °C, the dephosphorization ratio at the endpoint of dephosphorization rises to be above 55%, and the content of P₂O₅ in the dephosphorization slag is above 3.90%, with the excellent results of dephosphorization of hot metal.

3.3. Analysis of Dephosphorization Slag at the Optimum Dephosphorization Temperature of 1405 °C

Figure 4 shows the XRD analysis results of dephosphorization slag at 1405 °C. Figure 5 shows the images of dephosphorization slag by SEM-EDS at 1405 °C, with magnification of (a) 200 times and (b) 500 times, respectively. As shown in Figure 4, the dephosphorization slag is composed of dicalcium silicate Ca₂SiO₄, tricalcium silicate Ca₃SiO₄, phosphorus containing solid solution 6C₂S-C₃P, silicate phase Ca₃Mg(SiO₄)₂, calcium ferrite phase Ca₂Fe₂O₅, and oxide phase RO. It can be seen from Figure 5a that there is dark gray phase 1, gray phase 2, light gray phase 3, white phase 4, gray phase 5 and black phase 6 in the dephosphorization slag at the dephosphorization endpoint temperature of 1405 °C with the basicity of 1.64. Furthermore, SEM-EDS point analysis and map scanning were used to analyze the phase composition. Table 4 shows the elements compositions of different phases in dephosphorization slag by SEM-EDS point analysis in Figure 5a, and Figure 6 shows the map scanning results of dephosphorization slag at 1405 °C under the magnification of 200 times.

It can be seen from Table 4 that the phosphorus content in the dark gray phase 1-1, 1-2, and 1-3 is the highest, with an average value of 4.34%, followed by the phosphorus content in the gray phase 2-1, 2-2, and 2-3, with an average value of 3.44%, and the phosphorus content in the light gray phase 3, with the value of 2.20%. The contents of phosphorus in white phase 4, gray white phase 5, and black phase 6 were less than 1.5%. According to the XRD analysis results in Figure 4 and the map scanning results in Figure 6, it can be judged that the dark gray phase 1, the gray phase 2, and the light gray phase 3 are all phosphorus rich phases (P-rich phase), but their phosphorus enrichment degrees are different, and the order of phosphorus enrichment degree is the dark gray phase 1 > the gray phase 2 > the light gray phase 3. The content of Fe in the white phase 4 is very high, so it can be judged that the white phase 4 is the mixed iron particles. The gray white phase 5 has high contents

of Fe and Ca, which can be identified as $\text{Ca}_2\text{Fe}_2\text{O}_5$ by XRD analysis, which is named the Fe-rich phase. The black phase 6 contains a high content of Ca, Si, and a small amount of phosphorus. Therefore, the black phase 6 is considered as the matrix phase, which is known as the calcium silicate phase. From the SEM image of dephosphorization slag in Figure 5b, it is found that there are two kinds of Fe-rich phases in the dephosphorization slag at the dephosphorization endpoint temperature of 1405°C with the basicity of 1.64, which are petal-like and strip-like respectively. There are large P-rich phases in the slag with the size of more than $40\ \mu\text{m}$, and the calcium silicate phases are dispersed in small pieces between the P-rich phase and the Fe-rich phase.

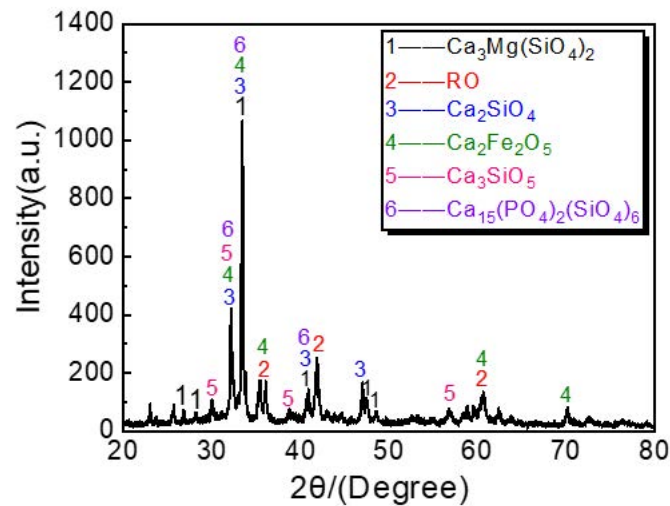


Figure 4. XRD analysis result of dephosphorization slag at 1405°C .

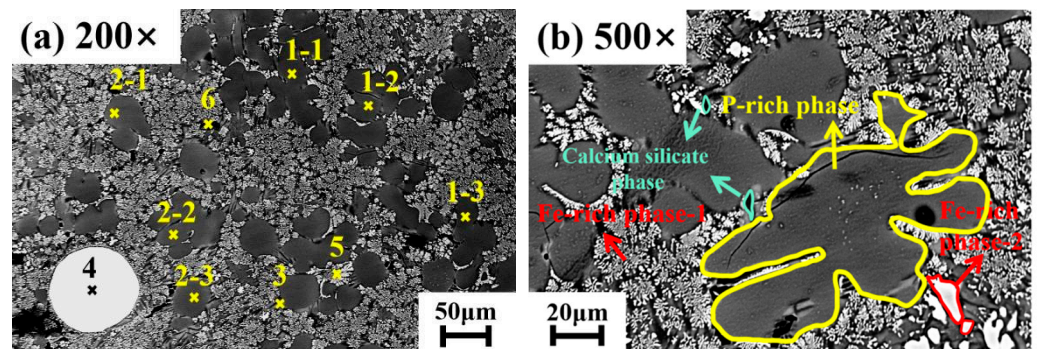


Figure 5. Images of dephosphorization slag by SEM-EDS at 1405°C of (a) 200 times; (b) 500 times.

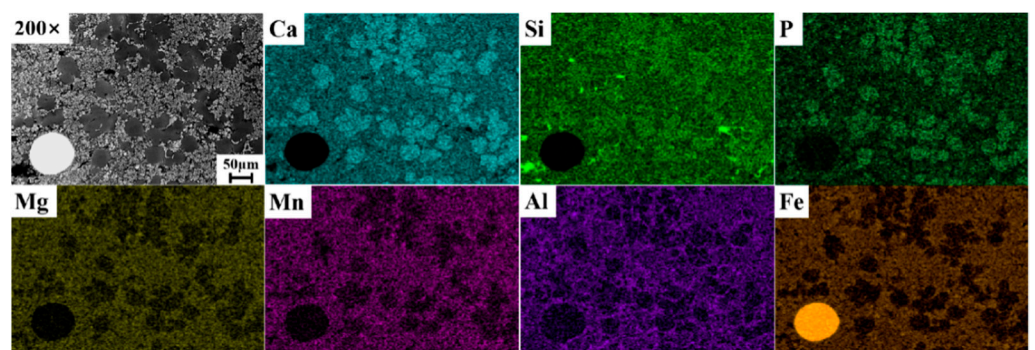


Figure 6. Element distribution results of dephosphorization slag at 1405°C .

Table 4. Element compositions of different phases in dephosphorization slag by SEM-EDS point analysis (mass%).

Position	Ca	Si	Mn	Mg	P	Al	Fe	O
1-1	34.77	12.94	2.70	2.03	4.34	0.16	1.62	41.44
1-2	35.98	12.37	2.90	2.08	4.25	0.12	1.26	41.04
1-3	37.00	13.93	3.63	1.36	4.42	0.01	2.22	37.43
2-1	29.68	13.23	3.39	2.94	3.61	1.65	2.65	42.85
2-2	35.25	13.80	2.18	1.99	3.51	0.14	1.58	41.55
2-3	29.06	13.27	3.78	2.19	3.20	2.13	3.16	43.21
3	30.56	12.55	6.02	2.49	2.20	0.85	5.80	39.53
4	2.32	0.92	3.55	1.35	0.17	0.43	82.14	9.12
5	20.36	10.22	7.33	2.92	1.14	2.03	24.06	31.94
6	27.08	17.79	3.19	3.33	1.44	2.56	4.15	40.46

3.4. Analysis of the P-Rich Phase in Dephosphorization Slag at 1405 °C

SEM-EDS was used to further analyze the boundary of the P-rich phase. Figure 7a,b show the P-rich phase in dephosphorization slag at 1405 °C with the magnifications of 1000 times and 2000 times, Figure 7c shows the schematic diagram of the P-rich phase boundary, and Figure 7d shows the schematic diagram of formation process of the P-rich phase. In Figure 7a,b, the gray massive phase is the P-rich phase, the gray white phase is the Fe-rich phase and the black phase is calcium silicate in dephosphorization slag. At the same time, it is found that the gray P-rich phase is surrounded by the black calcium silicate phase, and the outermost part is surrounded by a layer of the gray white Fe-rich phase. Furthermore, the P-rich phase of dephosphorization slag was observed at 2000 times magnification, and the size of different phases was measured by Image Pro Plus image software. It can be seen that the size of the P-rich phase is 45.31 μm , the width of the black calcium silicate phase wrapped outside is about 1.15 μm , and the width of the outermost gray white Fe-rich phase is about 0.74 μm .

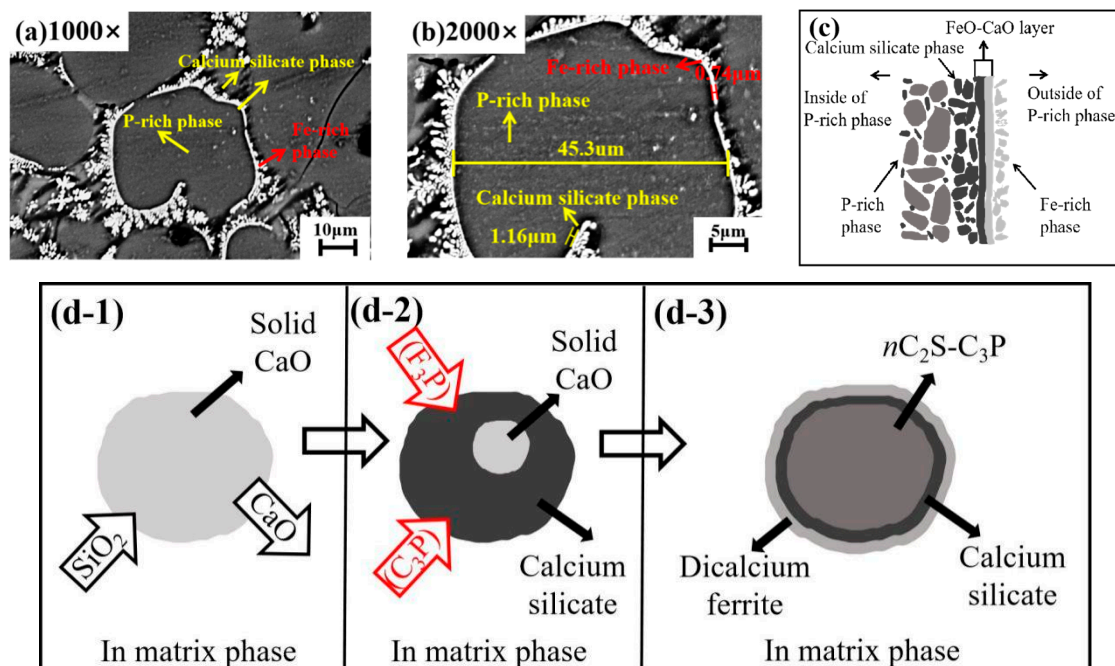


Figure 7. Images of the P-rich phase in dephosphorization slag at 1405 °C of (a) 1000 times; (b) 2000 times; (c) Schematic diagram of P-rich phase boundary; (d) Schematic diagram of formation process of the P-rich phase.

From Table 4, the content of phosphorus in the P-rich phase is higher than that in the calcium silicate phase, and the content of phosphorus in the calcium silicate phase is higher than that in the Fe-rich phase. Therefore, the enrichment path of phosphorus in hot metal can be reasonably inferred from the content gradient of phosphorus in the different phases, and the formation process of the P-rich phase was speculated, as shown in Figure 7d. The process from Figure 7(d-1) to (d-2) shows that the solid CaO particles in matrix phase will first form C_2S at the surface of CaO [20–22]. The process from Figure 7(d-2) to (d-3) shows that the phosphorus in hot metal is oxidized by iron oxide to form P_2O_5 and enters the slag, and FeO and CaO react with P_2O_5 to form $3FeO \cdot P_2O_5 (F_3P)$ and C_3P , respectively, which initially fixes phosphorus in dephosphorization slag. Since the F_3P is extremely unstable especially in the high temperature, CaO in slag will further react with F_3P to form the stable C_3P phase [23]. Finally, phosphorus exists in the P-rich phase in the form of nC_2S-C_3P solid solution. Since the dephosphorization slag is a multiphase slag with solid–liquid coexistence between 1350 and 1450 °C, there is undissolved calcium silicate solid phase in the slag. With the progress of the dephosphorization reaction, the phosphorus containing solid solution grows into the massive P-rich phase. The calcium silicate phase wrapped outside shrinks, and the corresponding FeO–CaO layer shrinks, finally forming the P-rich phase boundary, as shown in Figure 7c. Therefore, the path of phosphorus in hot metal entering the P-rich phase of dephosphorization slag can be reasonably inferred as: hot metal \rightarrow Fe-rich phase \rightarrow P-rich phase in dephosphorization slag.

4. Discussion

4.1. Effect of Dephosphorization Endpoint Temperature on a_{FeO} and P_{CO}^{P-C}

In the dephosphorization reaction, the iron oxide in slag acts as the main oxidant for dephosphorization. Therefore, the content of iron oxide in dephosphorization slag has a significant effect on the dephosphorization ability of dephosphorization slag. In this study, it is assumed that all iron oxides in slag exist in the form of FeO, so as to analyze the effect of dephosphorization endpoint temperature on a_{FeO} . It should be noted that the activity of each substance in the dephosphorization slag adopts pure substances as the standard state, and a_{FeO} in the dephosphorization slag is expressed as Equation (3) [24].

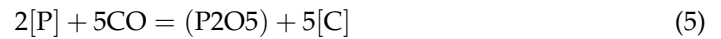
$$a_{FeO} = \gamma_{FeO} \times X_{FeO} \quad (3)$$

X_i is the mole fraction of oxide i in dephosphorization slag, and γ_i is the activity coefficient of oxide i . The present work uses the regular solution model to calculate γ_{FeO} , because this model can avoid the problem that the structure of the silicate anion changes with the number and type of cations and the temperature. In this model, it is assumed that various cations, such as Ca^{2+} , Fe^{2+} , Si^{4+} , and P^{5+} , are randomly distributed in the O^{2-} matrix, and O^{2-} is the common anion of various cations in the melt. According to the interaction energy between cations summarized by Ban-ya [25], γ_{FeO} can be expressed as Equation (4).

$$\begin{aligned} RT \ln \gamma_{FeO} = & 7110X_{MnO}^2 - 31,380X_{CaO}^2 + 33,470X_{MgO}^2 - 41,840X_{SiO_2}^2 - 31,380X_{P_2O_5}^2 \\ & - 41,000X_{Al_2O_3}^2 + 67,780X_{MnO}X_{CaO} - 21,410X_{MnO}X_{MgO} + 40,580X_{MnO}X_{SiO_2} \\ & + 60,670X_{MnO}X_{P_2O_5} + 49,790X_{MnO}X_{Al_2O_3} + 102,510X_{CaO}X_{MgO} + 60,670X_{CaO}X_{SiO_2} \\ & + 188,280X_{CaO}X_{P_2O_5} + 82,430X_{CaO}X_{Al_2O_3} + 58,570X_{MgO}X_{SiO_2} + 39,750X_{MgO}X_{P_2O_5} \\ & + 63,600X_{MgO}X_{Al_2O_3} - 156,900X_{SiO_2}X_{P_2O_5} + 45,130X_{SiO_2}X_{Al_2O_3} + 189,120X_{P_2O_5}X_{Al_2O_3} \end{aligned} \quad (4)$$

During the dephosphorization process of the converter, as the temperature of the hot metal rises and the dephosphorization reaction proceeds, carbon and phosphorus will undergo a selective oxidation transformation. The selective oxidation reaction of carbon and phosphorus is shown in Equation (5). Namely, when the temperature is lower than the selective oxidation temperature of carbon and phosphorus, the phosphorus in hot metal is preferentially oxidized. At the higher temperature, carbon is preferentially oxidized. The value of P_{CO} in a selective oxidation reaction of carbon and phosphorus is directly related to the selective oxidation temperature of carbon and phosphorus. Therefore, it is significant to

study the relationship between the partial pressure of CO and dephosphorization endpoint temperature in the selective oxidation of carbon and phosphorus for the dephosphorization of hot metal. In this paper, $P_{\text{CO}}^{\text{P-C}}$ is used to represent the partial pressure of CO in the selective oxidation of carbon and phosphorus.



$$\Delta G^\theta = -594,505 + 748.25T \quad (6)$$

$$K^\ominus = \frac{a_{\text{P}_2\text{O}_5} \times a_{[\text{C}]^5}}{P_{\text{CO}}^5 \times a_{[\text{P}]^2}} \quad (7)$$

Equation (6) is the Gibbs free energy of the carbon and phosphorus selective oxidation reaction (J). Equation (7) is the equilibrium constant expression of the reaction. P_2O_5 in dephosphorization slag adopts pure substance as the standard state. $a_{[\text{C}]}$ and $a_{[\text{P}]}$ represent the activities of carbon and phosphorus in hot metal, respectively. The standard state of the activity of $a_{[\text{C}]}$ and $a_{[\text{P}]}$ in hot metal is 1% mass fraction solution, which conforms to Henry's law. Therefore, $a_{[\text{C}]}$ and $a_{[\text{P}]}$ can be expressed by Equations (8) and (9). $a_{\text{P}_2\text{O}_5}$ is expressed as Equation (10).

$$a_{[\text{C}]} = f_{[\text{C}]} \times [\% \text{C}] \quad (8)$$

$$a_{[\text{P}]} = f_{[\text{P}]} \times [\% \text{P}] \quad (9)$$

$$a_{\text{P}_2\text{O}_5} = \gamma_{\text{P}_2\text{O}_5} \times X_{\text{P}_2\text{O}_5} \quad (10)$$

It should be noted that $\gamma_{\text{P}_2\text{O}_5}$ is calculated by empirical Equation (11) [26]. The reason for not using regular solution calculation is that the value of $a_{\text{P}_2\text{O}_5}$ in the actual slag is too small, usually smaller than 10^{-17} . [27] There is an error in the process of converting $a_{\text{P}_2\text{O}_5}$ to $a_{\text{P}_2\text{O}_5}$ obtained by the regular solution model, and the obtained $a_{\text{P}_2\text{O}_5}$ is far from the calculated values in previous studies. [28–30] Based on the above reasons, the empirical formula summarized by Turkdogan and Pearson is selected to calculate $\gamma_{\text{P}_2\text{O}_5}$ [26], and the activity coefficients of phosphorus and carbon in hot metal can be calculated by Equations (12) and (13).

$$\log \gamma_{\text{P}_2\text{O}_5} = -1.12(22X_{\text{CaO}} + 15X_{\text{MgO}} + 13X_{\text{MnO}} + 12X_{\text{FeO}} - 2X_{\text{SiO}_2}) - \frac{42,000}{T} + 23.58 \quad (11)$$

$$\log f_{[\text{P}]} = e_{\text{P}}^{\text{C}}[\% \text{C}] + e_{\text{P}}^{\text{Si}}[\% \text{Si}] + e_{\text{P}}^{\text{Mn}}[\% \text{Mn}] + e_{\text{P}}^{\text{S}}[\% \text{S}] + e_{\text{P}}^{\text{P}}[\% \text{P}] \quad (12)$$

$$\log f_{[\text{C}]} = e_{\text{C}}^{\text{C}}[\% \text{C}] + e_{\text{C}}^{\text{Si}}[\% \text{Si}] + e_{\text{C}}^{\text{Mn}}[\% \text{Mn}] + e_{\text{C}}^{\text{S}}[\% \text{S}] + e_{\text{C}}^{\text{P}}[\% \text{P}] \quad (13)$$

e_{P}^i and e_{C}^i are the interaction coefficients of solute element i to phosphorus and carbon dissolved in hot metal, respectively. With the progress of the dephosphorization reaction, a part of phosphorus in hot metal is fixed in dephosphorization slag and removed from hot metal. At the endpoint of dephosphorization stage in the double slag converter steelmaking process, it can be regarded that the dephosphorization quasi-equilibrium state is reached under the conditions of lower temperature and lower basicity. The value of a_{FeO} can be calculated by Equations (3) and (4), and the value of $P_{\text{CO}}^{\text{P-C}}$ can be calculated by Equations (6)–(13). Considering that a_{FeO} is mainly affected by the basic oxide contents in slag and the dephosphorization endpoint temperature, through the multiple linear regression on a_{FeO} , Equation (14) can be obtained with the regression coefficient R^2 of 0.97. Figure 8a shows the comparison between the predicted value based on multiple regression and the calculated value of a_{FeO} from the regular solution model of Equations (3) and (4). The predicted value is well consistent with the calculated result.

$$a_{\text{FeO}} = 0.0096 \times (\% \text{FeO}) - 0.004 \times (\% \text{CaO}) + 0.0026 \times (\% \text{MnO}) + 0.0134 \times (\% \text{MgO}) - 2.8923 \times 10^{-4} \times T + 0.5442 \quad (14)$$

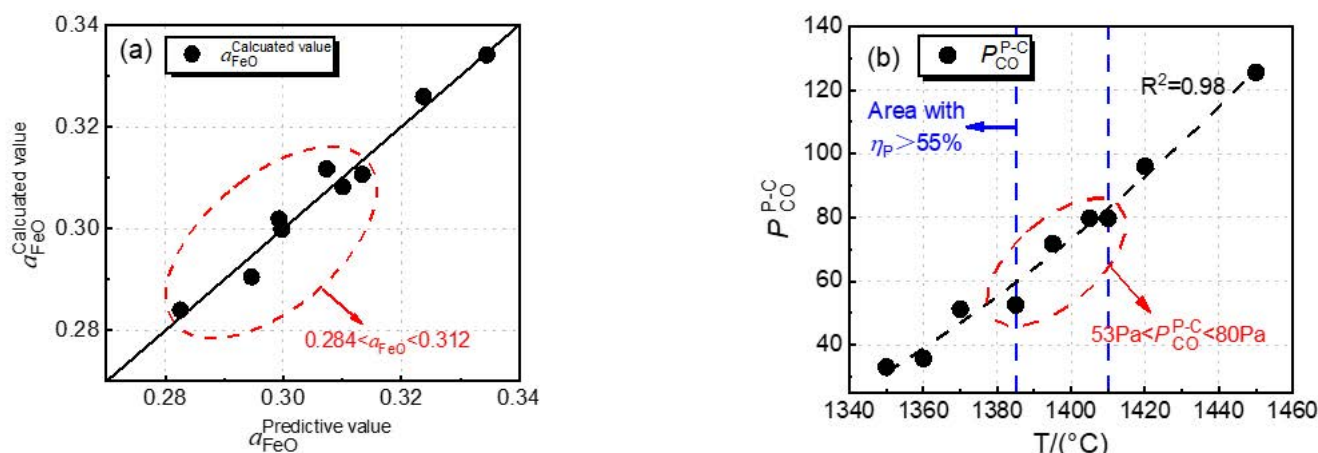


Figure 8. (a) Comparison between the predicted value based on multiple regression and the calculated value of a_{FeO} from the regular solution model; (b) Effect of dephosphorization endpoint temperature on P_{CO}^{P-C} of selective oxidation reaction of carbon and phosphorus.

Figure 8b shows the effect of dephosphorization endpoint temperature on P_{CO}^{P-C} of a selective oxidation reaction of carbon and phosphorus. In Figure 8b, P_{CO}^{P-C} data were fitted by an exponential curve, and the regression coefficient, R^2 , is 0.98, which indicates that there is a good exponential relationship between the endpoint temperature of dephosphorization and P_{CO}^{P-C} ; the fitting equation is shown in Equation (15). With increasing dephosphorization endpoint temperature, P_{CO}^{P-C} shows an exponential upward trend.

$$P_{CO}^{P-C} = 4.11 \times \exp\left(\frac{T - 576.82}{211.98}\right) - 126.41 \quad (15)$$

The blue dashed line area in Figure 8b shows that the dephosphorization ratio is greater than 55%, and the temperature range is 1385–1410 °C. In this range, the dephosphorization result is preferential, the P_{CO}^{P-C} value is 53–80 Pa, and a_{FeO} is 0.284–0.312. These two ranges are conducive to the dephosphorization of the converter.

4.2. Effect of Dephosphorization Endpoint Temperature on the Oxygen Activity on Hot Metal Surface, the Phosphorus Oxidation Equilibrium Oxygen Activity, and the Iron Oxidation Equilibrium Oxygen Activity at Slag–Hot Metal Interface

In the converter dephosphorization process, the oxygen in hot metal is mainly used to remove elements such as silicon, manganese, phosphorus, and carbon. Before dephosphorization reaches quasi equilibrium, with the decarburization reaction going on, the carbon in hot metal decreases continuously, and the carbon–oxygen reaction is in the state of excess oxygen. The equilibrium oxygen content in hot metal mainly depends on the carbon content in hot metal [16]. The carbon–oxygen reaction in the hot metal is shown in Equation (16), the Gibbs free energy of the reaction is expressed by Equation (17), and the equilibrium constant is given by Equation (18). It should be noted that P_{CO} in Equation (16) is the partial pressure of CO in the converter, and it is assumed to the value of 1 atm. In this paper, P_{CO}^{C-O} is used to represent the partial pressure of CO in the converter.



$$\Delta G^\theta = -22,200 - 38.34T \quad (17)$$

$$K^\ominus = \frac{P_{CO}^{C-O}}{a_{[C]} \times a_{[O]}} \quad (18)$$

Combined with Equations (16)–(18), the theoretical oxygen activity on the surface of hot metal of $a_{[O]}^{\text{iron}}$ can be deduced as shown in Equation (19).

$$\log a_{[O]}^{\text{iron}} = -\frac{1160}{T} - 2.002 + \log P_{\text{CO}}^{\text{C-O}} - \log a_{[C]} \quad (19)$$

At the slag–hot metal reaction interface, phosphorus in hot metal is oxidized to P_2O_5 , which enters slag and exists in the form of $\text{C}_2\text{S-C}_3\text{P}$ solid solution. The oxidative dephosphorization reaction occurs as Equation (20). Equation (21) is the equilibrium constant of dephosphorization reaction obtained by Turkdogan and Pearson [26], and Equation (22) is the expression of the equilibrium constant.



$$\log K = \frac{37,160}{T} - 29.67 \quad (21)$$

$$K^\ominus = \frac{a_{\text{P}_2\text{O}_5}}{a_{[\text{P}]}^2 \times a_{[\text{O}]}^5} \quad (22)$$

When the dephosphorization reaction of slag and hot metal reaches quasi equilibrium, by combining Equations (20)–(22), the oxygen activity of phosphorus oxidation at the slag–hot metal interface of $a_{[O]}^{\text{de[P]}}$ is derived as Equation (23).

$$\log a_{[O]}^{\text{de[P]}} = \left(-\frac{37,160}{T} + 29.67 + \log a_{\text{P}_2\text{O}_5} - 2 \log a_{[\text{P}]}\right) / 5 \quad (23)$$

The oxygen activity in the slag is mainly determined by the oxygen in the form of iron oxides. This article assumes that all iron oxides exist in the form of FeO , and the slag–hot metal interface reaches the quasi-equilibrium state of oxidation. Therefore, the oxygen activity of iron oxidation at the slag–hot metal interface can be expressed by the iron oxide reaction, as shown in Equation (24). The Gibbs free energy of reaction is shown in Equation (25) [24], and the equilibrium constant is shown in Equation (26).



$$\Delta G^\ominus = -128,090 + 57.990T \quad (25)$$

$$K^\ominus = \frac{a_{\text{FeO}}}{a_{[\text{O}]} \times a_{[\text{Fe}]}} \quad (26)$$

The concentration of $[\text{Fe}]$ in hot metal is very high, and the value of $a_{[\text{Fe}]}$ is taken as 1. When the iron oxidation reaction at the slag–hot metal interface reaches quasi equilibrium, by combining Equations (3), (4), and (26), the oxygen activity of the iron oxidation at the slag–hot metal interface of $a_{[O]}^{[\text{Fe}]-[\text{O}]}$ is obtained as shown in Equation (27).

$$\log a_{[O]}^{[\text{Fe}]-[\text{O}]} = -\frac{6689.77}{T} + 3.029 + \log a_{\text{FeO}} \quad (27)$$

The effect of the dephosphorization endpoint temperature on oxygen activity at different reaction interfaces in the dephosphorization stage of the converter is calculated by using Equations (19), (23), and (27), as shown in Figure 9a. It can be seen from Figure 9a that $a_{[O]}^{\text{de[P]}}$ and $a_{[O]}^{[\text{Fe}]-[\text{O}]}$ both increase with increasing dephosphorization endpoint temperature as a whole, while $a_{[O]}^{\text{iron}}$ first increases and then decreases. These results can be explained by the thermodynamic principle. The main decarburization reaction in steelmaking is Equation (16), which is an exothermic reaction. With dephosphorization endpoint temperature from 1350 to 1410 °C, the carbon–oxygen product increases; under the condition of little change in carbon content, the $a_{[O]}^{\text{iron}}$ and $a_{[O]}^{\text{de[P]}}$ increase rapidly [31]. When the

dephosphorization endpoint temperature is 1410–1450 °C, the dephosphorization reaction is weakened, the oxygen content of reaction with phosphorus is reduced, the phosphorus content increases from 0.051% to 0.103%, and the carbon content increases from 2.94% to 3.49% in hot metal, so the $a_{[O]}^{\text{iron}}$ decreases, and $a_{[O]}^{\text{de[P]}}$ increases slowly. Since $a_{[O]}^{[\text{Fe}]-[\text{O}]}$ is mainly affected by the iron oxide content in slag and temperature, $a_{[O]}^{[\text{Fe}]-[\text{O}]}$ increases with the increase of temperature when the iron oxide content does not change obviously.

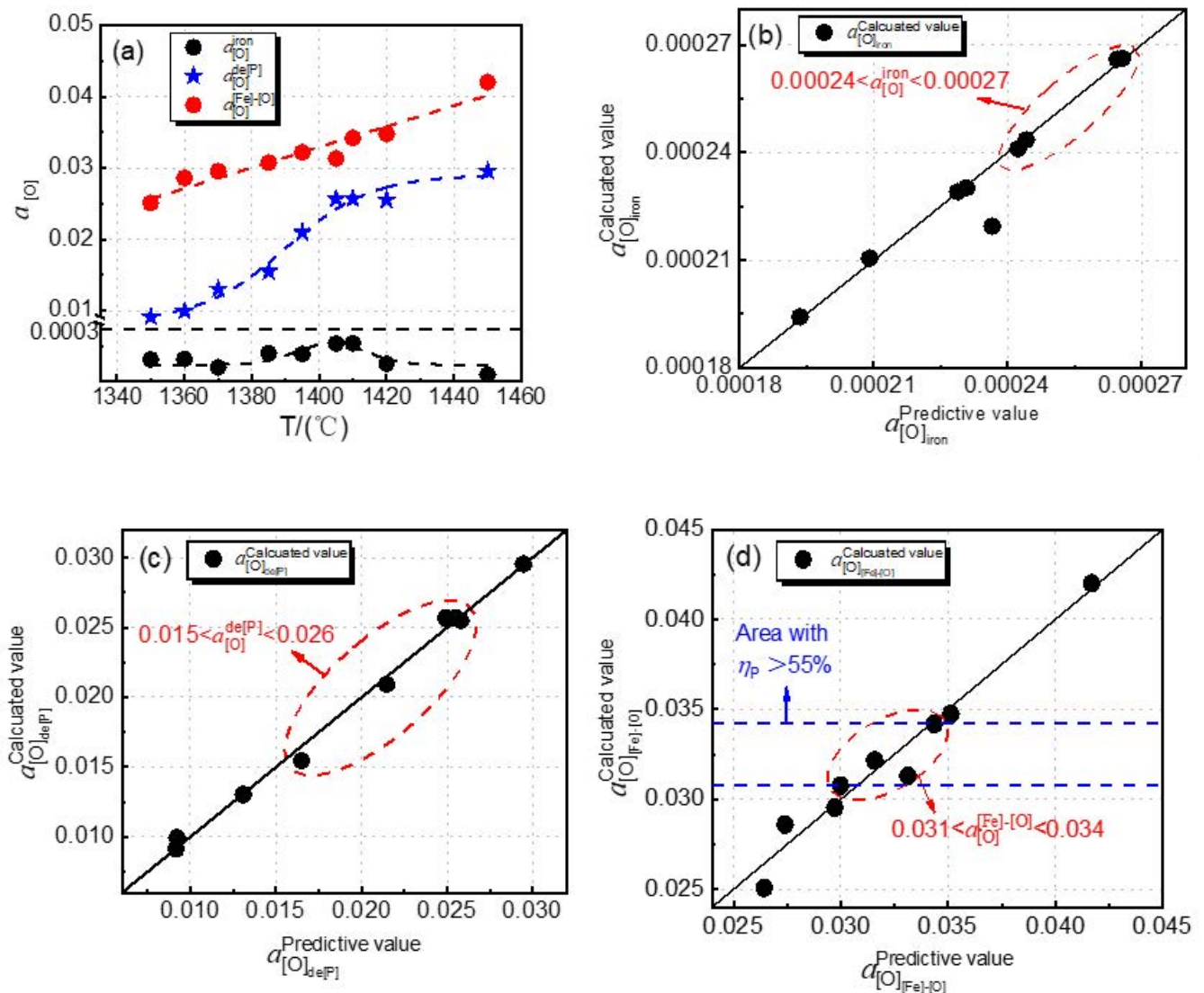


Figure 9. (a) Effect of dephosphorization endpoint temperature on $a_{[O]}^{\text{iron}}$, $a_{[O]}^{\text{de[P]}}$, and $a_{[O]}^{[\text{Fe}]-[\text{O}]}$; Comparison between predicted value and calculated value based on multiple regression, (b) $a_{[O]}^{\text{iron}}$; (c) $a_{[O]}^{\text{de[P]}}$; (d) $a_{[O]}^{[\text{Fe}]-[\text{O}]}$.

According to the different reaction interfaces of dephosphorization in the converter, the relationships between $a_{[O]}^{\text{iron}}$, $a_{[O]}^{\text{de[P]}}$, $a_{[O]}^{[\text{Fe}]-[\text{O}]}$, the dephosphorization endpoint temperature, and the compositions of hot metal and slag are fitted by multiple linear regression, which are expressed as Equations (28)–(30), respectively. It is found that the values of $a_{[O]}$ calculated by Equations (19), (23), and (27) all have a good multiple linear relationship with the regression coefficients, R^2 , of 0.99, 0.97, and 0.96, respectively.

$$a_{[O]}^{\text{iron}} = -1.529 \times 10^{-4} \times [\%C] + 2.7657 \times 10^{-7} \times T + 3.258 \times 10^{-4} \quad (28)$$

$$a_{[O]}^{\text{de}[P]} = -0.00211 \times (\%P_2O_5) - 0.131 \times [\%P] + 2.423 \times 10^{-4} \times T - 0.3017 \quad (29)$$

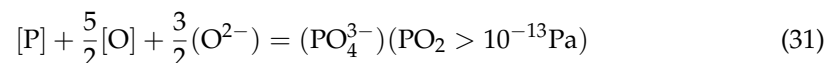
$$a_{[O]}^{[Fe]-[O]} = 1.7046 \times 10^{-4} \times T + 0.00125 \times (\%FeO) - 0.2274 \quad (30)$$

It can be seen from Figure 9a that the increase trend of $a_{[O]}^{\text{de}[P]}$ is slightly faster, and the growth trends of $a_{[O]}^{\text{iron}}$ and $a_{[O]}^{[Fe]-[O]}$ are slightly slower in the temperature range of 1350–1405 °C, which indicates that the effect of temperature on the phosphorus oxygen equilibrium of the slag–hot metal interface is relatively large in the temperature range of 1350–1405 °C. The increase trend of $a_{[O]}^{[Fe]-[O]}$ is slightly faster in the temperature range of 1405–1450 °C, which indicates that the temperature has a greater effect on the iron oxygen equilibrium in the slag in temperature range of 1405–1450 °C.

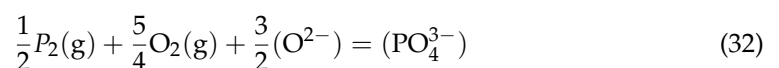
In the range of 1350–1450 °C, $a_{[O]}^{[Fe]-[O]} > a_{[O]}^{\text{de}[P]} > a_{[O]}^{\text{iron}}$. The results show that $a_{[O]}^{[Fe]-[O]}$ is the highest, while $a_{[O]}^{\text{iron}}$ is the lowest, which is consistent with the research results of Kitamura. [17] Since there is a large amount of Fe in the dephosphorization process, the oxygen activity at the slag–hot metal interface mainly depends on the oxygen activity in equilibrium with iron. According to the analysis in Figure 9, $a_{[O]}^{[Fe]-[O]}$ plays a major role in the dephosphorization reaction in the range of 1350–1450 °C. Since the temperature range of the high dephosphorization ratio is 1385–1410 °C, $a_{[O]}^{[Fe]-[O]}$ should be between 0.031 and 0.034.

4.3. Effect of Dephosphorization Endpoint Temperature on Phosphorus Capacity and Phosphorus Distribution Ratio of Dephosphorization Slag

The solubility of phosphorus in molten slag can be expressed by phosphorus capacity, which is an important indicator of the potential dephosphorization capacity of slag. During the dephosphorization process of hot metal, the phosphorus that is oxidized and transferred to slag mainly exists in the form of phosphate ion PO_4^{3-} . According to the theory of ion dephosphorization, the formation reaction of PO_4^{3-} is Equation (31) [32].



Wagner proposed the concept of phosphate capacity $C_{PO_4^{3-}}$ based on the gas–slag equilibrium; the reaction expression is Equation (32), which is expressed as Equation (33) [33]. Yang et al. [32,34] defined the phosphorus capacity index, $C_{PO_4^{3-}\text{-index}}$, which is based on slag–metal equilibrium. The reaction expression is Equation (31), with $C_{PO_4^{3-}\text{-index}}$ expressed as Equation (34). The deduced relationship between $C_{PO_4^{3-}}$ and $C_{PO_4^{3-}\text{-index}}$ can be expressed as Equation (35), and it can be applicable to any slag system [34].



$$C_{PO_4^{3-}} = \frac{(\%PO_4^{3-})}{P_2^{1/2} O_2^{5/4}} \quad (33)$$

$$C_{PO_4^{3-}\text{-index}} = \frac{(\%PO_4^{3-})}{a_{[P]} \times (a_{[O]})^{5/2}} \quad (34)$$

$$\log C_{PO_4^{3-}} = \log C_{PO_4^{3-}\text{-index}} + \frac{23,531.25}{T} + 0.1606 \quad (35)$$

In Equations (33) and (34), (%PO₄³⁻) is the phosphate content in the slag, and the relationship between (%PO₄³⁻) and (%P₂O₅) is shown in Equation (36) [32,34].

$$(\%PO_4^{3-}) = \frac{2MPO_4^{3-}}{MP_2O_5} (\%P_2O_5) = 1.3382(\%P_2O_5) \tag{36}$$

M_i represents the molecular weight of oxide *i*. The expression of log C_{PO₄³⁻} is obtained by combining Equations (27) and (33)–(36), as shown in Equation (37).

$$\log C_{PO_4^{3-}} = \log \frac{1.3382(\%P_2O_5)}{a_{[P]} \times (a_{[O]}^{[Fe]-[O]})^{5/2}} + \frac{23,531.25}{T} + 0.1606 \tag{37}$$

In Equation (37), a_[P] is calculated by Equation (11). Iron oxide is the main oxidant in the dephosphorization process. According to the discussion in Section 4.2, the oxygen activity in the slag is mainly determined by the oxygen activity of the iron oxidation equilibrium at slag–hot metal interface. Therefore, a_[O] in Equation (37) is calculated by using a_[O]^{[Fe]-[O]} in Equation (27).

The empirical formulas for calculating log C_{PO₄³⁻} are listed in Table 5, where Λ represents the optical basicity of the slag, which is expressed as Equation (38). x_i is the mole fraction of cations in oxide *i*, which is expressed as Equation (39). n_i is the number of oxygen atoms in oxide *i* and x'_i is the mole fraction of oxide *i*. Table 6 lists the optical basicities of various oxides [28].

$$\Lambda = \sum x_i \Lambda_i \tag{38}$$

$$x_i = \frac{n_i(O)x'_i}{\sum n_i(O)x'_i} \tag{39}$$

Table 5. Empirical formulas of log C_{PO₄³⁻}.

Scholar	Slag	Empirical Formulas
Yang [28]	CaO-FeO-SiO ₂ -MgO-Al ₂ O ₃	log C _{PO₄³⁻} = 19.4Λ + 6.74
Maruoka [35]	CaO-FeO-SiO ₂ -MgO-Al ₂ O ₃	log C _{PO₄³⁻} = 20.67Λ + 66,204/T - - - 32.01
Selin [36]	CaO-SiO ₂ -CaF ₂	log C _{PO₄³⁻} = 2.016 $\frac{(x_{CaO})}{(x_{SiO_2})}$ 0.34 $\left(\frac{(x_{CaO})}{(x_{SiO_2})}\right)^2$ + 52,600/T 11.506
Sobandi [37]	CaO-MnO-SiO ₂ -PO _{2.5} (-MgO, Fe _t O)	log C _{PO₄³⁻} = 2.60{ (%CaO) + 0.33(%MnO) + 0.55(%MgO) 0.90(%Fe _t O)0.77(%PO _{2.5}) } / (%SiO ₂) + 40,400/T6.48

Table 6. Optical basicities of different oxides.

Oxide	CaO	SiO ₂	MnO	P ₂ O ₅	FeO	Fe ₂ O ₃	MgO	Al ₂ O ₃
Λ	1.00	0.46	0.59	0.40	0.51	0.48	0.78	0.60

Figure 10 shows the comparison of log C_{PO₄³⁻} between the calculated value of the empirical formulas and the calculated value in this paper at different dephosphorization endpoint temperatures. log C_{PO₄³⁻} in Figure 10 is calculated by Equation (37) and different empirical formulas in Table 5. It can be concluded that the calculated values of log C_{PO₄³⁻} from the empirical formulas of Maruoka et al. [35], Selin et al. [36], and Sobandi et al. [37] all decrease with increasing dephosphorization endpoint temperature, and the changing trend is similar, which is consistent with the thermodynamic result that the increase in temperature is not conducive to the dephosphorization of hot metal. The calculated values of log C_{PO₄³⁻} from Yang’s empirical formula do not change with the increasing dephosphorization endpoint temperature significantly. This is because Yang et al. [28] mainly studied the effect of dephosphorization slag basicity on phosphorus capacity, and

the optical basicity plays a decisive role in their empirical formula. The calculated values of $\log C_{\text{PO}_4^{3-}}$ in the present work show a trend of first decreasing, then increasing, and then decreasing again. The value of the calculated results at 1385–1410 °C in the present work are consistent to those of Yang et al. [24]. This is because the experimental temperature, dephosphorization slag basicity, and composition in the present work are similar to the experimental temperature of 1380 °C, slag basicity of 1.40–1.83, and slag compositions of CaO-MnO-MgO-SiO₂-P₂O₅-Fe_tO-Al₂O₃ in their paper, and they did the laboratorial experiments based on the double slag steelmaking process.

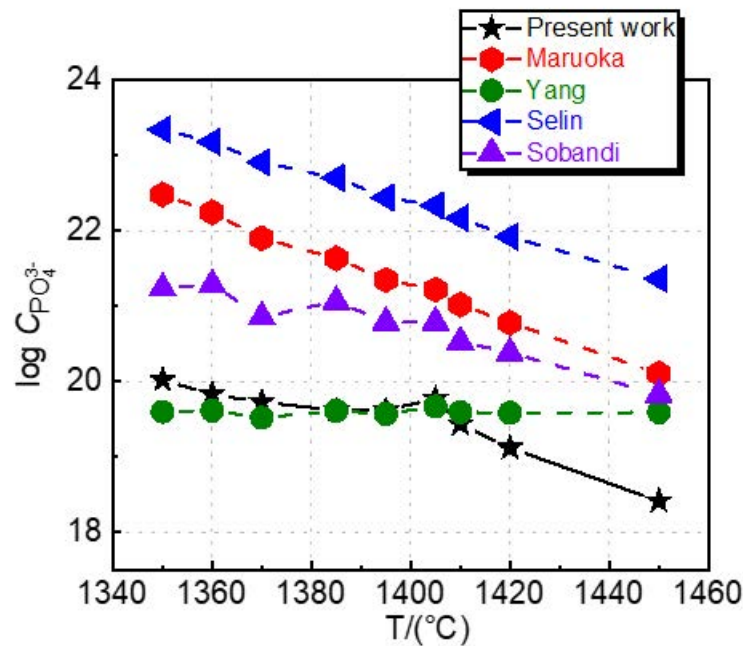


Figure 10. Comparison of $\log C_{\text{PO}_4^{3-}}$ between the calculated value of the empirical formulas and the calculated value in this paper at different dephosphorization endpoint temperatures.

The calculated results in the present work are smaller than those calculated by the empirical formulas, which become smaller when the temperature is increased. This is because most of the formulas in Table 6 are the results of laboratory equilibrium under ideal experimental conditions. However, the dephosphorization reaction has not reached equilibrium value due to the short time of dephosphorization in the industrial experiment, which is only about 5 min. Therefore, the $\log C_{\text{PO}_4^{3-}}$ value calculated in the present work is smaller than those calculated by empirical formulas.

From Equations (12), (27), and (37), Equation (40) of the phosphorus distribution ratio $\log L_P$ based on the oxygen activity of iron oxidation equilibrium at the slag-hot metal interface can be deduced as follows:

$$\log L_P = \log C_{\text{PO}_4^{3-}} + \log f_P + \frac{5}{2} \log a_{[\text{O}]}^{\text{[Fe]}-\text{[O]}} - 23,531.25/T - 0.287 \quad (40)$$

Figure 11 shows the comparison of $\log L_P$ between the calculated values of the empirical formulas and the calculated values in this paper at different dephosphorization endpoint temperatures. The values of $\log L_P$ in Figure 11 are calculated by Equation (40) and the different empirical formulas in Table 7. According to Figure 11, all empirical formulas indicate that the values of $\log L_P$ show a downward trend at first, then an upward trend around 1405 °C, and then a downward trend again with increasing dephosphorization endpoint temperature. The $\log L_P$ value calculated by the Ogawa formula is the closest to the calculated results in the present paper. It is noticed that between 1395 and 1410 °C, the $\log L_P$ values calculated by the Ogawa formula are consistent with the calculated values in

the present work. This is because the Ogawa formula is based on the formula summarized in the dephosphorization stage of the typical double slag converter steelmaking process—the MURC process. Therefore, the temperature and basicity used in the Ogawa formula are similar to those in the present paper. In addition, the effect of the higher [%C] content in hot metal on L_P is taken into consideration, so that it is suitable for the dephosphorization of hot metal with the higher carbon content in the dephosphorization stage of the present work. This is consistent with our previous results on the double slag converter steelmaking process [4].

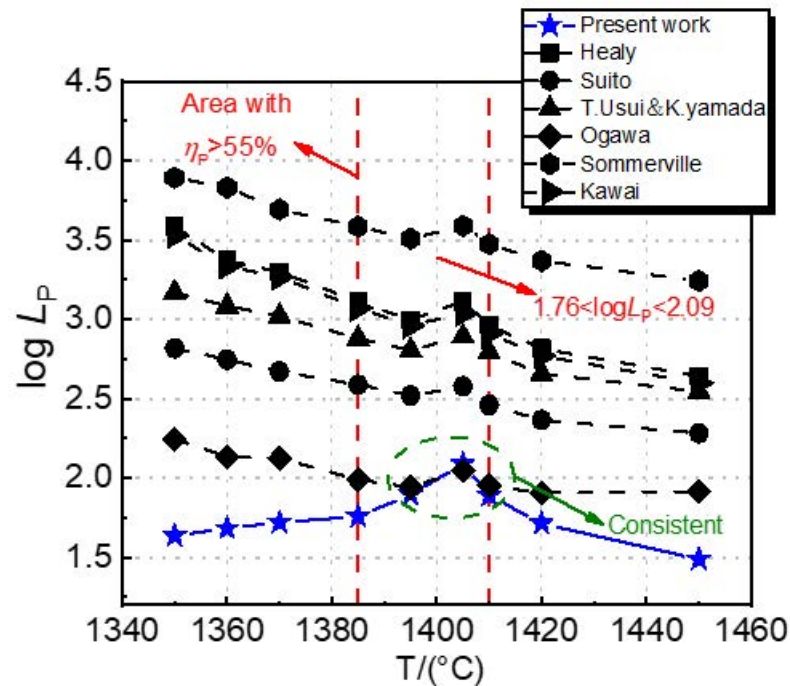


Figure 11. Comparison of $\log L_P$ between the calculated value of the empirical formulas and the calculated values in this paper at different dephosphorization endpoint temperatures.

Table 7. Empirical formulas of $\log L_P$.

Scholar	Slag	Empirical Formulas
Healy [38]	CaO-SiO ₂ -Fe _t O-P ₂ O ₅	$\log L_P = \log \frac{(\%P)}{[\%P]} = 22,350/T - 24.0 + 7 \log (\%CaO) + 2.5 \log (\%T.Fe)$ ($(\%CaO) \geq 30$)
		$\log L_P = \log \frac{(\%P)}{[\%P]} = 22,350/T - 16.0 + 0.08 (\%CaO) + 2.5 \log (\%T.Fe)$ ($(\%CaO) < 30$)
Suito [39]	CaO-SiO ₂ -Fe _t O-P ₂ O ₅ -MgO-MnO	$\log L_P = \log \frac{(\%P)}{([\%P](\%T.Fe)^{5/2})} = 0.072[(\%CaO) + 0.3(\%MgO) + 0.6(\%P_2O_5) + 0.6(\%MnO)] + 2.5 \lg (\%T.Fe) + 11,570/T - 10.52$
Kawai [40]	CaO-SiO ₂ -Fe _t O-P ₂ O ₅	$\log L_P = \log \frac{(\%P)}{[\%P]} = 22,350/T - 21.876 + 5.6 \log (\%CaO) + 2.5 \log (\%T.Fe)$
T.Usui&K.Yamada [41]	CaO-Fe _t O-SiO ₂ -P ₂ O ₅ -MgO-Al ₂ O ₃ -TiO ₂	$\log L_P = 5.60 \log [(\%CaO) + 0.3(MgO) + 0.05(\%Fe_tO)] + 14,800/T - 18.038 + 0.5 \log (\%P_2O_5) + 2.5 \log (\%Fe_t)$
Ogawa [1]	CaO-SiO ₂ -Fe _t O-P ₂ O ₅ -MgO-MnO	$\log L_P = \log \frac{(\%P)}{[\%P]} = 2.5 \log (\%T.Fe) + 0.0715\{(\%CaO) + 0.25(\%MgO)\} + 7710/T - 8.55 + (105.1/T + 0.0723) [\%C]$
Zhang [42]	CaO-SiO ₂ -FeO-P ₂ O ₅ -MgO-MnO	$\log L_P = \log \frac{(\%P_2O_5)}{[\%P]} = [162(\%CaO) + 127.5(\%MgO) + 28.5(\%MnO)]/T + 2.5 \lg (\%FeO) - 6.287 \times 10^{-4} \times \log (\%SiO_2)^2 + 11,000/T - 10.4$

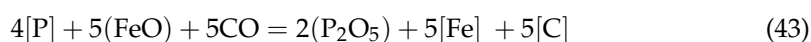
It can be seen from Figure 11 that with the increasing dephosphorization endpoint temperature, the calculated results in the present work show $\log L_P$ first rising and then

decreasing obviously, which is consistent with the changing trend of the dephosphorization ratio in Figure 3. When the dephosphorization endpoint temperature is in the range of 1350–1405 °C, with increasing temperature, the auxiliary materials such as lime and dolomite are easy to melt, so that the kinetic conditions of dephosphorization are improved. Although increasing temperature is unfavorable to the thermodynamic conditions of dephosphorization, the overall L_P still increases, and the dephosphorization result shows an upward trend. When the endpoint temperature of dephosphorization exceeds 1405 °C, with further increasing the temperature, the equilibrium constant of the dephosphorization reaction decreases greatly, and the dephosphorization ratio decreases, resulting in a decrease in L_P .

The calculated values of $\log L_P$ in the present work are closer to the empirical formula values of Ogawa et al. [1], but they are lower than the empirical formula values of the others, because the empirical formulas of Healy et al. [38], Suito et al. [39], Usui and Yamada et al. [41], and Zhang et al. [42] were from an equilibrium dephosphorization reaction under laboratorial experiments and not for the double slag process. The empirical formula of Kawai et al. [40] was from the industrial experiments but not for the double slag process. The empirical formula of Ogawa et al. [1] was for the double slag process. However, their dephosphorization times were up to 8 min, and their experiments were carried out in an 8 t converter so that the dephosphorization reaction could be carried out close to the equilibrium results. According to the results in Figure 11, the optimum dephosphorization temperature is in the range of 1385–1410 °C and the optimum $\log L_P$ value is in the range of 1.76–2.09.

4.4. Effect of Dephosphorization Endpoint Temperature on Dephosphorization, Rephosphorization, and the Optimum Temperature of Deslagging

According to previous scholars on the double slag converter steelmaking industrial experimental research, it is necessary to study the optimum temperature of intermediate deslagging theoretically [18,43,44]. As the desiliconization and dephosphorization reactions proceed, the converter temperature increases gradually. Since phosphorus in hot metal is oxidized by FeO and reduced by carbon at the same time, combining the dephosphorization reaction Equation (41) of oxidation of P by FeO and the rephosphorization reaction Equation (42) of the reduction of P_2O_5 by C, the coupling dephosphorization reaction among FeO, C, and P can be obtained as Equation (43). The Gibbs free energy expression of the reaction is taken from the literature [18]. Equation (46) is obtained from Equations (44) and (45).



$$\Delta G_{FeO-P} = -27,763.36 + 255.23T + RT \ln \left(\frac{a_{P_2O_5}}{a_{FeO}^5 \times a_{[P]}^2} \right) \quad (44)$$

$$\Delta G_{C-P_2O_5} = 521,758.34 - 709.02T + RT \ln \left(\frac{(P_{CO}^{P-C})^5 \times a_{[P]}^2}{a_{P_2O_5} \times a_{[C]}^5} \right) \quad (45)$$

$$\Delta G_{FeO-CO-P} = -549,521.71 + 964.26T + RT \ln \left(\frac{a_{P_2O_5}^2 \times a_{[C]}^5}{P_{CO}^5 \times a_{[P]}^4 \times a_{FeO}^5} \right) \quad (46)$$

Figure 12 shows the effect of dephosphorization endpoint temperature on the actual Gibbs free energy (ΔG) changes of FeO-P, C- P_2O_5 , and FeO-CO-P reactions. The ΔG values of the three reactions of FeO-P, C- P_2O_5 , and FeO-CO-P are calculated from Equations (44)–(46), where $a_{P_2O_5}$ is calculated from Equations (10) and (11), P_{CO}^{P-C} is calculated by Equations (6)–(13), $a_{[C]}$, $a_{[P]}$ and a_{FeO} are calculated by Equations (8) and (9), and Equations (3) and (4), respectively.

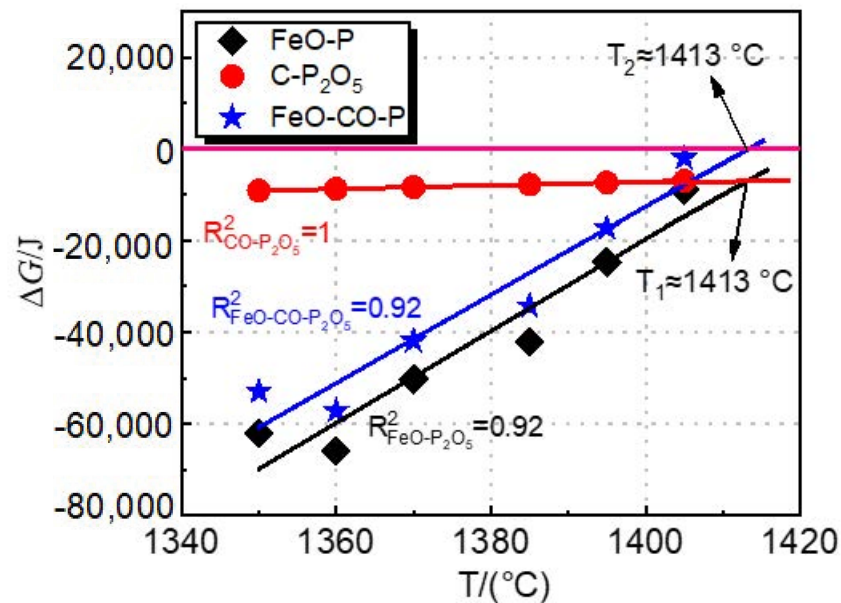


Figure 12. Effect of dephosphorization endpoint temperature on the actual Gibbs free energy changes of FeO-P, C-P₂O₅, and FeO-CO-P reactions.

It can be seen from Figure 12 that the ΔG values of FeO-P and C-P₂O₅ are both smaller than 0, which means that in the dephosphorization stage with the temperature in the range of 1350–1405 °C, both the dephosphorization reaction of phosphorus oxidation by FeO and rephosphorization reaction of reduction of P₂O₅ by carbon occur. With the increasing dephosphorization endpoint temperature, the ΔG value of the C-P₂O₅ reaction does not change significantly, which indicates that temperature has little effect on rephosphorization in 1350–1405 °C.

The ΔG values of the three reactions are linearly fitted with the dephosphorization endpoint temperature, with the regression coefficients, R^2 , are 0.92, 0.99, and 0.92, respectively. The fitting line of the C-P₂O₅ ΔG value and the fitting line of the FeO-P ΔG value cross when T_1 is about 1413 °C, which means the oxidation of phosphorus by FeO and the reduction of P₂O₅ by carbon are in dynamic equilibrium at this temperature. At the temperature lower than 1413 °C, dephosphorization and rephosphorization reactions are carried out simultaneously in the converter, and the trend of dephosphorization reaction is greater than that of rephosphorization. When the temperature is higher than T_1 , the trend of the rephosphorization reaction in the converter will be greater than that of the dephosphorization reaction, resulting in the rephosphorization of hot metal.

Figure 12 also shows the result of Equation (46) obtained by coupling Equations (44) and (45), as shown by the blue line in the Figure 12. The ΔG value of the FeO-CO-P reaction increases with the increasing dephosphorization endpoint temperature. When the temperature T_2 exceeds 1413 °C, the ΔG is greater than 0. The trend of rephosphorization in the FeO-CO-P coupling dephosphorization reaction is greater than that of dephosphorization.

It can be seen from Figure 12 that the temperature T_2 at which the ΔG value of the FeO-CO-P reaction is 0 is the same as T_1 . It shows that the FeO-CO-P coupled dephosphorization reaction is equivalent to combining the dephosphorization reaction and the rephosphorization reaction. Considering the experimental results and thermodynamic calculation results of industrial experiments by the double slag dephosphorization process, the optimal temperature range for intermediate deslagging is about 1400–1420 °C.

5. Conclusions

In the present work, the industrial experiments of dephosphorization in the double slag converter steelmaking process under the conditions of low temperature and low basicity were carried out. The effect of dephosphorization endpoint temperature on the dephosphorization of hot metal was studied, and the following conclusions were drawn:

- (1) In the temperature range of 1350–1450 °C, with increasing dephosphorization endpoint temperature, the dephosphorization ratio and phosphorus distribution ratio first increase and then decrease. The phosphorus content in hot metal at the end of dephosphorization first decreases and then increases. The optimum dephosphorization temperature is in the range of 1385–1410 °C, with the dephosphorization ratio higher than 55%, the P₂O₅ content in the dephosphorization slag of 3.93–4.17%, and the logL_P value of 1.76–2.09.
- (2) Dephosphorization slag is mainly composed of the gray massive P-rich phase, gray white Fe-rich phase, and black calcium silicate phase. The path of phosphorus in hot metal entering the P-rich phase of dephosphorization slag can be reasonably inferred as: hot metal → Fe-rich phase → P-rich phase in dephosphorization slag.
- (3) a_{FeO} is decided by the dephosphorization endpoint temperature and basic oxide content in dephosphorization slag, and a_{FeO} has multiple linear correlation with them. The $P_{\text{CO}}^{\text{P-C}}$ of selective oxidation reaction of carbon and phosphorus has a good exponential relationship with the endpoint temperature of dephosphorization. It is beneficial to converter dephosphorization when the temperature is 1385–1410 °C, the value of $P_{\text{CO}}^{\text{P-C}}$ is 53–80 Pa, and a_{FeO} value is 0.284–0.312.
- (4) The oxygen activity on the surface of hot metal of $a_{[\text{O}]}^{\text{iron}}$, the oxygen activity of the phosphorus oxidation at the slag–hot metal interface of $a_{[\text{O}]}^{\text{de[P]}}$, and the oxygen activity of the iron oxidation at the slag–hot metal interface of $a_{[\text{O}]}^{[\text{Fe}]-[\text{O}]}$ all increase with increasing the dephosphorization endpoint temperature in the range of 1350–1405 °C. The temperature has the greater effect on the phosphorus oxygen equilibrium of the slag–hot metal interface in the temperature range of 1350–1405 °C, and the temperature has a greater effect on the iron oxygen equilibrium in the slag in the temperature range of 1405–1450 °C. In the temperature range of 1350–1450 °C, owing to $a_{[\text{O}]}^{[\text{Fe}]-[\text{O}]} > a_{[\text{O}]}^{\text{de[P]}} > a_{[\text{O}]}^{\text{iron}}$, $a_{[\text{O}]}^{[\text{Fe}]-[\text{O}]}$ plays the most important role on the dephosphorization in the double slag steelmaking process.
- (5) Under the present industrial experimental conditions, when the temperature is 1413 °C, the dephosphorization and rephosphorization reactions are in dynamic equilibrium. Considering the experimental results and thermodynamic calculation results of industrial experiments by the double slag dephosphorization process, the optimal temperature range for intermediate deslagging is about 1400–1420 °C.

Author Contributions: Conceptualization, H.S. and J.Y.; methodology, J.Y.; validation, X.L. and W.L.; formal analysis, H.S.; investigation, H.S.; resources, X.L. and W.L.; data curation, W.Y., G.Y., R.Z. and H.S.; writing—original draft preparation, H.S.; writing—review and editing, J.Y.; visualization, H.S.; supervision, J.Y.; project administration, J.Y.; funding acquisition, J.Y. All authors have read and agreed to the published version of the manuscript.

Funding: This work is financially supported by the National Natural Science Foundation of China (Grant No. U1960202).

Data Availability Statement: Data supporting reported results can be found in this paper.

Acknowledgments: The authors would like to thank the National Natural Science Foundation of China (Grant No. U1960202). The equipment was partially provided by the State Key Laboratory of Advanced Special Steel, School of Materials Science and Engineering, Shanghai University.

Conflicts of Interest: The authors declare no conflict of interest.

References

1. Ogawa, Y.; Yano, M.; Kitamura, S.; Hirata, H. Development of the Continuous Dephosphorization and Decarburization Process Using BOF. *Tetsu-to-Hagane* **2001**, *87*, 21–28. [[CrossRef](#)]
2. Wang, Y.; Yang, S.; Li, J.; Feng, J.; Wang, F. Dephosphorization by Double-Slag Process in Converter Steelmaking. *High Temp. Mater. Process.* **2017**, *37*, 625–633. [[CrossRef](#)]
3. Wu, H.; Li, J.; Zhou, C.G.; Cai, K.S.; Wu, G.P.; Cai, Y.L. Practice on first deslagging process of double slag dephosphorization in 120 t top and bottom combined blown converter. *Spec. Steel* **2013**, *34*, 30–32.
4. Ye, G.-F.; Yang, J.; Zhang, R.-H.; Yang, W.-K.; Sun, H. Behavior of phosphorus enrichment in dephosphorization slag at low temperature and low basicity. *Int. J. Miner. Met. Mater.* **2021**, *28*, 66–75. [[CrossRef](#)]
5. Kobayashi, Y.; Yiming, T.; Takahashi, S.; Endo, R. Thermal Conductivity of 2CaO-SiO₂ Bearing Solid Solution. *ISIJ Int.* **2017**, *57*, 1698–1702. [[CrossRef](#)]
6. Kitamura, S.-Y.; Shibata, H.; Maruoka, N. Kinetic Model of Hot Metal Dephosphorization by Liquid and Solid Coexisting Slags. *Steel Res. Int.* **2008**, *79*, 586–590. [[CrossRef](#)]
7. Suito, H.; Inoue, R. Behavior of phosphorous transfer from CaO-Fe₁O-P₂O₅(-SiO₂) slag to CaO particles. *ISIJ Int.* **2006**, *46*, 180–187. [[CrossRef](#)]
8. Kitamura, S.Y.; Saito, S.; Utogawa, K.; Shibata, H.; Robertson, D.G. Mass transfer of P₂O₅ between liquid slag and solid solution of 2CaO-SiO₂ and 3CaO-P₂O₅. *ISIJ Int.* **2009**, *49*, 1838–1844. [[CrossRef](#)]
9. Xie, S.; Wang, W.; Luo, Z.; Huang, D. Mass Transfer Behavior of Phosphorus from the Liquid Slag Phase to Solid 2CaO-SiO₂ in the Multiphase Dephosphorization Slag. *Met. Mater. Trans. A* **2016**, *47*, 1583–1593. [[CrossRef](#)]
10. Kakimoto, S.; Kiyose, A.; Murao, R. Influence of P₂O₅ on dissolution behavior of lime in molten slag. *ISIJ Int.* **2017**, *49*, 1710–1717. [[CrossRef](#)]
11. Wu, X.R.; Wang, P.; Li, L.S.; Wu, Z.J.; Chen, R.H. Distribution and enrichment of phosphorus in solidified BOF steelmaking slag. *Ironmak. Steelmak.* **2011**, *38*, 185–188. [[CrossRef](#)]
12. Pahlevani, F.; Kitamura, S.Y.; Shibata, H.; Maruoka, N. Distribution of P₂O₅ between solid solution of 2CaO-SiO₂-3CaO-P₂O₅ and liquid phase. *ISIJ Int.* **2010**, *50*, 822–829. [[CrossRef](#)]
13. Tian, Z.H.; Li, B.H.; Zhang, X.M.; Jiang, Z.H. Double slag operation dephosphorization in BOF for producing low phosphorus steel. *J. Iron Steel Res. Int.* **2009**, *16*, 6–14. [[CrossRef](#)]
14. Yang, X.; Sun, F.-M.; Yang, J.-L.; Liu, F.; Cheng, K.-S.; Wang, J.-H. Optimization of Low Phosphorus Steel Production with Double Slag Process in BOF. *J. Iron Steel Res. Int.* **2013**, *20*, 41–47. [[CrossRef](#)]
15. Zhou, C.G.; Li, J.; Wu, H.; Yang, K.Z.; Cai, K.S.; Wu, G.P.; Cao, Y.L. Study of factors affecting liquid steel rephosphorization. *Iron Steel Vanadium Titan.* **2014**, *35*, 116–122.
16. Han, X.; Li, J.; Hu, X.G.; Zhou, C.G.; Zhang, H.Y.; Guo, C. Effect of oxidability of final slag in converter on dephosphorization. *Foundry Technol.* **2015**, *36*, 412–415.
17. Kitamura, S.Y.; Yonezawa, K.; Ogawa, Y.; Sasaki, N. Improvement of reaction efficiency in hot metal dephosphorization. *Ironmak. Steelmak.* **2002**, *29*, 121–124. [[CrossRef](#)]
18. Zhou, C.G.; Li, J.; Wu, H.; Cai, K.S.; Wu, G.P.; Cao, Y.L. Study on the temperature of first deslagging of double slag dephosphorization in converter. *Iron Steel* **2014**, *49*, 24–28.
19. Karbowniczek, M.; Cebula, E.K.; Reichel, J. Investigations of the dephosphorization of liquid iron solution containing chromium and nickel mater. *Met. Mater. Trans. B* **2012**, *43*, 554–561. [[CrossRef](#)]
20. Hamano, T.; Fukagai, S.; Tsukihashi, F. Reaction mechanism between solid CaO and FeOx-CaO-SiO₂-P₂O₅ slag at 1573 K. *ISIJ Int.* **2006**, *46*, 490–495. [[CrossRef](#)]
21. Yang, X.; Matsuura, H.; Tsukihashi, F. Condensation of P₂O₅ at the interface between 2CaO center dot SiO₂ and CaO-SiO₂-FeO_x-P₂O₅ slag. *ISIJ Int.* **2009**, *49*, 1298–1307. [[CrossRef](#)]
22. Yang, X.; Matsuura, H.; Tsukihashi, F. Reaction Behavior of P₂O₅ at the interface between solid 2CaO center dot SiO₂ and liquid CaO-SiO₂-FeO_x-P₂O₅ slags saturated with solid 5CaO center dot SiO₂ center dot P₂O₅ at 1573 K. *ISIJ Int.* **2010**, *50*, 702–711. [[CrossRef](#)]
23. Xie, S.; Wang, W.; Huang, D.; Li, H.; Du, Y. Clarification of the Dissolution of Solid CaO and the Phosphorus-Enrichment Capability of Calcium Silicates in the Multiphase Slag Based on the Ion and Molecule Coexistence Theory. *Steel Res. Int.* **2018**, *89*. [[CrossRef](#)]
24. Huang, X.H. *Principles of Iron and Steel Metallurgy*; Metallurgical Industry Press: Beijing, China, 2002; pp. 213–215.
25. Ban-Ya, S. Mathematical Expression of Slag-Metal Reactions in Steelmaking Process by Quadratic Formalism Based on the Regular Solution Model. *ISIJ Int.* **1993**, *33*, 2–11. [[CrossRef](#)]
26. Turkdogan, E.T.; Pearson, J. Activities of constituents of iron and steelmaking slags, Part 3-Phosphorus pentoxide. *Iron Steel* **1953**, *175*, 398–403.
27. Yang, X.M.; Duan, J.P.; Shi, C.B.; Zhang, M.; Zhang, Y.L.; Wang, J.C. A thermodynamic model of phosphate distribution ratio between CaO-SiO₂-MgO-FeO-Fe₂O₃-MnO-Al₂O₃-P₂O₅ slags and molten steel during a top-bottom combined blown converter steelmaking process based on the ion and molecule coexistence theory. *Met. Mater. Trans. B* **2011**, *42*, 738–770. [[CrossRef](#)]
28. Yang, W.; Yang, J.; Shi, Y.; Yang, Z.; Gao, F.; Zhang, R.; Ye, G. Effect of basicity on dephosphorization of hot metal with a low basicity slag at 1653 K. *Ironmak. Steelmak.* **2021**, *48*, 69–77. [[CrossRef](#)]

29. Turkdogan, E.T. Assessment of P₂O₅ Activity Coefficients in Molten Slags. *ISIJ Int.* **2000**, *40*, 964–970. [[CrossRef](#)]
30. Basu, S.; Lahiri, A.K.; Seetharaman, S. A Model for Activity Coefficient of P₂O₅ in BOF Slag and Phosphorus Distribution between Liquid Steel and Slag. *ISIJ Int.* **2007**, *47*, 1236–1238. [[CrossRef](#)]
31. Wu, X.; Bao, Y.P.; Yue, F.; Feng, J.; Tang, D.C. Study on factors to affect the product of carbon content and oxygen content at blowing end-point of BOF steelmaking. *Res. Iron Steel* **2010**, *38*, 26–29.
32. Yang, X.M.; Li, J.Y.; Chai, G.M.; Duan, D.P.; Zhang, J. A thermodynamic model for predicting phosphate capacity of CaO-based slags during hot metal dephosphorization pretreatment process. *Ironmak. Steelmak.* **2017**, *44*, 437–454. [[CrossRef](#)]
33. Wagner, C. The concept of the basicity of slags. *Met. Mater. Trans. A* **1975**, *6*, 405–409. [[CrossRef](#)]
34. Yang, X.M.; Shi, C.B.; Zhang, M.; Duan, J.P.; Zhang, J. A thermodynamic model of phosphate capacity for CaO-SiO₂-MgO-FeO-Fe₂O₃-MnO-Al₂O₃-P₂O₅ slags equilibrated with molten steel during a top-bottom combined blown converter steelmaking process based on the ion and molecule coexistence theory. *Met. Mater. Trans. B* **2011**, *42*, 951–976. [[CrossRef](#)]
35. Maruoka, N.; Ono, S.; Kitamura, S.Y. Equilibrium distribution ratio of phosphorus between solid iron and magnesio-wustite-saturated Al₂O₃-CaO-Fe_tO-MgO-SiO₂ slag at 1623K. *ISIJ Int.* **2013**, *53*, 1709–1714. [[CrossRef](#)]
36. Roger, S.; Dong, Y.C.; Wu, Q.A. Uses of limes-based fluxes for simultaneous removal of phosphorus and sulfur in hot metal pretreatment. *Scand. J. Met.* **1990**, *19*, 98–109.
37. Sobandi, A.; Katayama, H.G.; Momono, T. Activity of phosphorus oxide in CaO-MnO-SiO₂-PO_{2.5}(-MgO, Fe_tO) slags. *ISIJ Int.* **1998**, *38*, 781–788. [[CrossRef](#)]
38. Healy, G.W. A new look at phosphorus distribution. *Iron Steel* **1970**, *208*, 664–668.
39. Suito, H.; Inoue, R. Phosphorus distribution between MgO-saturated CaO-Fe_tO-SiO₂-P₂O₅-MnO slags and liquid iron. *Trans. ISIJ* **1984**, *24*, 40–46. [[CrossRef](#)]
40. Kawai, Y.; Takahashi, I.; Miyashita, Y.; Tachibana, K. For dephosphorization equilibrium between slag and molten steel in the converter furnace. *Tetsu-to-Hagané* **1977**, *63*, 156.
41. Usui, T.; Yamada, K.; Kawai, Y.; Inoue, S.; Ishikawa, H.; Nimura, Y. Experiment of phosphorus and oxygen distribution between CaO-SiO₂-MgO-Fe_tO slag and liquid steel and estimation of phosphorus content at end point of top and bottom blowing converter. *Tetsu-to-Hagané* **1991**, *77*, 1641–1648. [[CrossRef](#)]
42. Zhang, X.F.; Sommerville, I.D.; Toguri, J.M. Equation for the equilibrium distribution of phosphorus between basic slags and steel. *Trans. Iron Steel Soc.* **1985**, *6*, 29–35.
43. Zhou, C.G.; Li, J.; Luo, K.M.; Han, X.; Zhang, Z.M.; Liu, Z.M.; Deng, C.F. First deslagging practice of double slag process for dephosphorization. *Iron Steel Vanadium Titan.* **2016**, *37*, 119–126.
44. Zhang, T.X.; Song, J.S.; Zhou, D.D.; Liu, X.Y. Calculation and process test for dephosphorization parameter of 120t converter. *Spec. Steel* **2020**, *41*, 25–27.